Comprehensive analysis of strong-field ionization and dissociation of diatomic nitrogen

John P. Nibarger, Saipriya V. Menon, and George N. Gibson
Department of Physics, University of Connecticut, Storrs, Connecticut 06269
(Received 24 August 2000; published 13 April 2001)

Accurate potential-energy curves are used consistently instead of Coulombic curves to determine the internuclear separation at ionization, R_{ion}, in a strong laser field, for charge states of N_2 up to N_2^{5+}. Furthermore, we exlude the kinetic energy gained from previous ionization steps in determining R_{ion}. With these improvements, we analyze various dissociation pathways from N_2^{2+} to N_2^{5+} and find that the charge symmetric pathways do not give physical results. In fact, it appears that *all* ionization up to N_2^{5+} involves the charge asymmetric channel $N_2^{4+} \rightarrow N^+ + N^{3+}$. By determining the time between each ionization step, we observe the competition between laser intensity and internuclear separation in determining the molecular ionization rate. Finally, our data are consistent with recent observations that short pulse (<130 fs) ionization leaves fragments in electronically excited states whereas long pulse (>600 fs) ionization leaves them in ground electronic states.

DOI: 10.1103/PhysRevA.63.053406 PACS number(s): 33.80.Rv, 33.80.Wz, 42.50.Hz

I. INTRODUCTION

Amplified, short pulse Ti:sapphire lasers can create strong electric fields that ionize and dissociate diatomic molecules. Compared to atoms, molecules exhibit complex behavior, arising from their additional degrees of freedom, such as symmetric and asymmetric dissociation [1–5], alignment with an external field [6–8], creation of electronically excited fragments [9,10], and ionization rates that depend on the internuclear separation [11–14].

From the earliest experiments on molecules in strong fields, much attention has been focused on measuring the kinetic energy release from the dissociation of molecules of different charge states. This energy release has been used to deduce the initial internuclear separation of the ions, R_{ion}, by assuming the energy comes from the potential energy of the Coulomb repulsion of the charges. Interestingly, this internuclear separation at the moment of ionization was measured to be nearly the same for all charge states of a given molecule and was called ''*R*-critical'' or R_C [2]. More significantly, R_C was found to be approximately two to three times the equilibrium separation of the neutral molecule, R_E, *for all homonuclear diatomic molecules and over a wide range of laser pulse durations.*

Theoretical explanations for these observations quickly followed with calculations by Seideman *et al.* [11], Chelkowski and Bandrauk [15], and Zuo *et al.* [16,17] (for a recent review, see [18]) showing that the ionization rate of a diatomic molecule has a strong dependence on internuclear separation and can increase by orders of magnitude at R_C. Thus, when the molecule reaches R_C, ionization rapidly occurs to high charge states and all charge states appear to dissociate from the same internuclear separation. Theoretical work on this problem has continued to the present [4,12–14,19], but all confirm the basic fact that the ionization rate peaks strongly at R_C. A variety of experiments have also shown the importance of R_C [20,21].

Despite the success of understanding the kinetic energy released based on the role of R_C, several issues remain unresolved. First, how does the molecule initially expand to R_C? Bond softening provides such a mechanism in H_2^+ [21–23 making this a clean system to study the ionization rates around R_C. For heavier molecules, it was generally assumed that the expansion takes place on a repulsive curve of a low charge state. However, this has not been demonstrated in detail. This issue has even led to a completely new explanation for the ''energy deficit'' problem [24–26]. Second, recent experiments by Yamanouchi *et al.* [27] raise the question of whether R_C is different for even and odd charged molecules. This has been accompanied by recent theoretical work as well [28], which demonstrates that enhanced ionization in even charged molecules occurs through a completely different mechanism than odd charged molecules. Third, charge asymmetric dissociation plays an important, if not dominant role in strong field dissociation of molecules [5,29,30]. However, there has been no theoretical work predicting the internuclear separation for ionization to charge asymmetric channels. Furthermore, it appears that the charge asymmetric channels come from smaller internuclear separations than their corresponding symmetric channels [5,30], raising the possibility that the symmetric channels, in fact, come from the asymmetric channels. Finally, a quite startling observation has been reported in the literature for several years now, which challenges even our most basic understanding of molecules in strong laser fields: highly charged molecules, such as Cl_2^{6+}, appear to be stable against dissociation in the presence of a strong laser field [31,32].

Although the existence of R_C seems to explain certain aspects of the strong field ionization of molecules, the general lack of a coherent picture motivated us to reexamine the underlying assumptions for determining R_{ion} from the kinetic energy releases. In particular, we wanted to address two of the questions raised above: how does a molecule initially start to expand and does charge asymmetric dissociation really occur at a smaller internuclear separation than the symmetric channels? Furthermore, we also wanted to find a consistent picture for the whole sequence of ionization steps from the neutral molecule to the highest charge state we could observe. This is significant because, in atoms, successive ionization steps are basically decoupled except for the rather weak multielectron ionization [33]. In molecules, however, the steps are tightly coupled because the ionization rate depends strongly on both the laser intensity and the in-

ternuclear separation and both of these quantities change rapidly during ionization.

In this paper, we present data and an analysis of the strong field ionization and dissociation of N_2 with ultrashort (33 fs) laser pulses. In the past, measured kinetic energy has been converted directly to R_{ion} using Coulomb potential energy curves, with the exception of Hill *et al.* [34]. This approach contained no information about the pathway to the final ionization state or the details of the potential energy curves. Instead, we base our analysis on accurate potential energy curves rather than the Coulombic approximation, as well as taking into account the entire dissociation pathway to properly keep track of all the contributions to the kinetic energy release of a particular charge state. We compare alternative ionization pathways to the higher charge states. Finally, we also determine the time from one ionization step to the next.

Our results show, that the molecule steadily grows in size from its equilibrium separation as it is ionized through the various charge states. However, we do observe a competition between the increasing ionization rate due to the increasing field and due to the increasing internuclear separation. This has led us to the hypothesis that ionization dominated by increasing laser intensity leaves fragments in electronically excited states, whereas ionization dominated by internuclear separation enhancement results in ground-state fragments.

II. EXPERIMENTAL SETUP

An Ar^+ laser pumped Kerr lens mode-locked Ti:sapphire oscillator was used to seed an eight-pass amplifer [35] pumped by a Nd:YLF laser. The output was a 400 μJ pulse at a repetition rate of 1 kHz, center frequency of 800 nm, and a pulse duration of 33 fs full width at half maximum (FWHM) fitted to a Gaussian. The pulse duration was measured with a real-time second-harmonic autocorrelator.

A vacuum chamber with a base pressure $<5\times10^{-10}$ torr was effusively filled with nitrogen gas to typical pressures of 10^{-9}–10^{-6} torr. A standard time of flight (TOF) geometry was used [Fig. 1(a)] to measure charge states and kinetic energies. The laser pulses were focused by an on-axis parabolic mirror into the extraction region where an additional grid, the field flattening grid in Fig. 1(b), was used to minimize the electrostatic lensing at the pinhole. The importance of the field flattening grid is that the electric field at the laser focus is better defined than in a simple extraction region with only two grids, improving our measurement of the kinetic energies. For instance, in a dissociation involving $N_2{}^{4+} \rightarrow N^+ + N^{3+}$, the N^+ fragment would be more susceptible to differences in the electric field than the N^{3+}. [Hereafter, we will label $N_2^{n+m} \rightarrow N^{n+} + N^{m+}$ as the (n,m) channel, where n is the detected ion.] This can lead to differences in the measured kinetic energy of the (3,1) dissociation in the 3^+ spectrum and the (1,3) dissociation in the 1^+ spectrum. As will be seen, the field-flattening grid greatly improved the agreement between these measurements.

Following the extraction region was a set of ion optics which include horizontal and vertical steering plates and a lens. Symmetric TOF dispersion was achieved by adjusting the ratio of extraction to acceleration voltages.

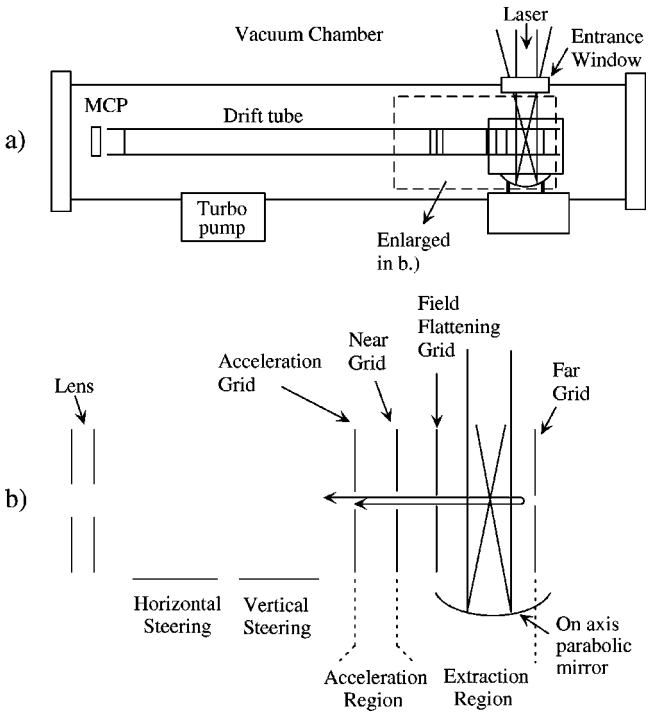

FIG. 1. (a) Time of flight chamber. (b) Detail of electrostatic grids.

The ions were measured using a microchannel plate (MCP) with an acceleration voltage of 2000 V and whose output was attenuated by 5 dB before going into a broadband 1 gigahertz 100× amplifier. After the amplifier, the signal was sent to a constant fraction discriminator and then to a 16-bit time-to-digital converter (TDC). The detector was kept from saturation by insuring that data were taken at a maximum rate of 1 ion/shot into the TDC. Intensity calibration of the laser was done routinely with an Ar^+ ion yield and yields a peak intensity of 1.1×10^{15} W/cm^2 [36].

III. DATA ACQUISITION

Taking data that are not influenced by detector saturation and space charge is extremely important for accurate kinetic energy measurements. We can minimize these factors through control of the nitrogen gas pressure. Space charge is due to the plasma created at the focus of the laser. After the escape of the electrons, ions located at the periphery are submitted to a repulsive electrostatic force depending on the number of ions in the focal region [3], increasing their measured kinetic energy. In our data, space charge is eliminated by taking spectra at a variety of different pressures and extrapolating the measured kinetic energy to the limit of zero pressure. Detector saturation is controlled by lowering the pressure to keep the count rate below 1 count/shot. For low signals, up to 100 000 laser shots were used to improve the statistics on the spectrum.

Typical data are shown in Fig. 2. The (n,n) peaks were identified through correlations, while the other peaks in each charge state were determined by counting the peaks on either side. The energies of the peaks identified in this way are

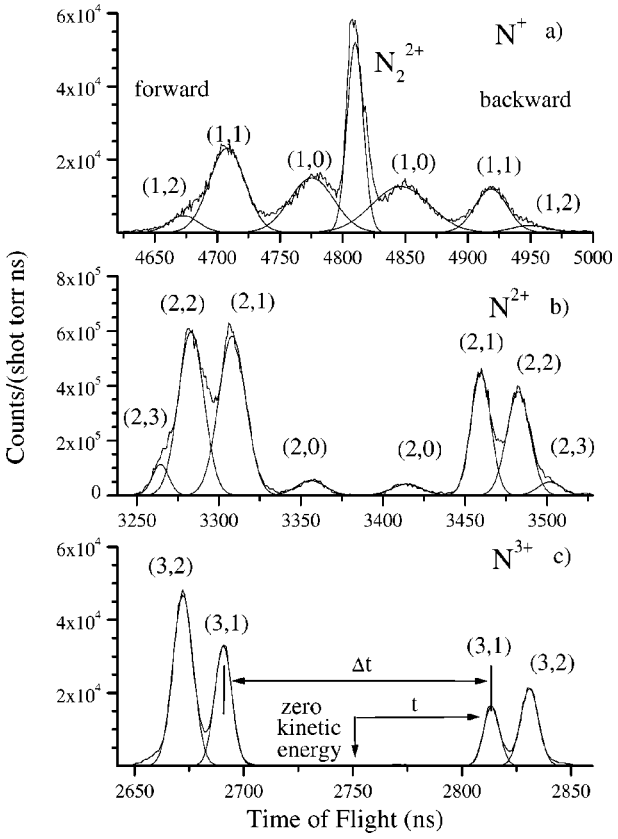

FIG. 2. Spectra with the identified forward (ions initially directed towards the detector) and backward (ions initially directed away from the detector) peaks fit with a multiple Gaussian: (a) N^+, (b) N^{2+}, and (c) N^{3+}. The N^{3+} spectrum also shows the timing of the peaks used to calculate their kinetic energy.

consistent with previously reported results [1–5,30,37,38]. We did not correlate other peaks directly because of the lack of dynamic range. For instance, in trying to find correlations for the (3,1) peak we found that when data were taken on the N^{3+} spectrum at a sufficient high pressure for good statistics, the N^+ spectrum was totally saturated. Similarly, when the pressure was optimal for the N^+ spectrum, the counting rate for the N^{3+} spectrum was too low for accurate statistics.

The energy of the dissociation was found using two methods. The first is to fit both the forward and backward peaks to a Gaussian function and calculate the total energy by using the time difference between the forward and backward peaks ($\triangle t$):

$$E = k(\triangle t)^2, \tag{1}$$

where $k = q^2F^2/8m$, F is the applied electric field in the extraction region, m is the mass of the fragment, and q is the charge of the fragment. The error in $\triangle t$ is found by adding the standard deviation of the centers of the two peaks in quadrature.

The second method more properly involves fitting the spectrum with a Gaussian function in time and then transforming the spectrum to energy. The transformation is more easily carried out on the time delay from zero kinetic energy, t. Because we have a symmetric TOF, $\triangle t = 2t$ (Fig. 2), giving

$$E(t) = 4kt^2 \tag{2}$$

which can be inverted to find $t(E)$:

$$t(E) = \sqrt{\frac{E}{4k}}. \tag{3}$$

The signal in time is found by fitting the spectra to a Gaussian function with width ω, centered at t_c:

$$S(t, t_c, \omega) = e^{-\{[t(E) - t_c]/\omega\}^2}. \tag{4}$$

The conversion from t to E is given by $S(E, t_c, \omega)dE = S(t, t_c, \omega)dt$. The Jacobian of the transformation is found from Eq. (3):

$$\frac{dt}{dE} = \sqrt{\frac{1}{4kE}}, \tag{5}$$

giving

$$S(E, t_c, \omega) = \sqrt{\frac{1}{4kE}} e^{-\{[\sqrt{(E/4k)} - t_c]/\omega\}^2}. \tag{6}$$

The energy for a given peak can be found by solving for E from

$$\frac{S(E, t_c, \omega)}{dE} = 0 \tag{7}$$

which yields the single-particle energy as a function of the measured parameters, ω and t_c, from the TOF specta:

$$E(t_c, \omega) = 2k(t_c^2 - \omega^2) + 2kt_c\sqrt{2\omega^2 + t_c^2}. \tag{8}$$

A comparison of the two methods is shown in Fig. 3. For the lowest dissociation energy of 1.2 eV for the (1,0) channel the error was 3.8%, but for the (1,1) dissociation energy of 7.8 eV the error was only 0.3%. Although the error can become significant for very low energies, we only use energies from the (1,1) channel and higher. Since the error is small we take advantage of Eq. (1) and measure only the time difference ($\triangle t$) of the peaks to calculate the dissociation energy.

To ensure that the data were not affected by space charge and detector saturation, data were taken for each dissociation channel at various pressures. Figure 4 shows the data that were taken for the (3,1) channel. These data were then extrapolated to zero pressure to determine the final dissociation energy. This was done for all the dissociation channels as a function of laser intensity as shown in Fig. 5. We see that there is agreement of the measured energy within error bars of the (1,2) with (2,1), (1,3) with (3,1), and (2,3) with (3,2).

IV. METHODS OF DATA ANALYSIS

The observation from Fig. 5 that the dissociation energy is a function of laser intensity has not been reported previously

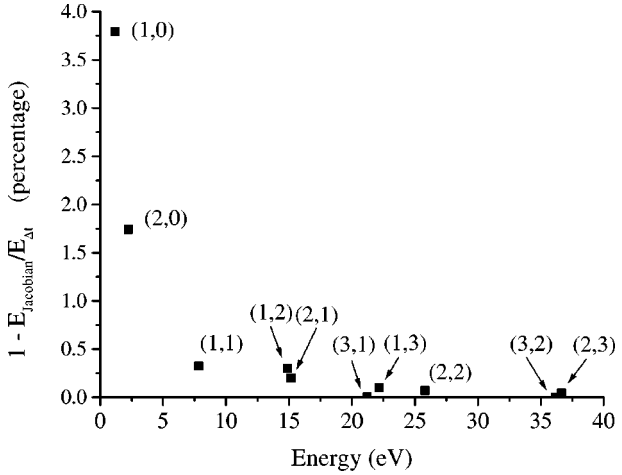

FIG. 3. Percentage error as a function of observed channel energy between energy calculated using the Jacobian transformation, E_{Jacobian} [Eq. (8)], and calculated solely using the time difference ($\triangle t$), $E_{\triangle t}$ [Eq. (1)].

in the literature. Detailed calculations on the ionization of Cl_2 in a strong laser field [15] would lead to such an observation and is the most likely explanation. Because of this variation, we need to decide the appropriate dissociation energy to use for each channel. We use two methods for the comparison of different channels: constant laser intensity and constant ion yield. The method of cutting the data using constant peak laser intensity is experimentally straightforward. It is done by finding the dissociation energy for each channel at a fixed peak laser intensity and is the method generally used in previous studies. However, cuts of constant peak laser intensity correspond to measuring each dissociation fragment (n,m) at a different intensity. This is due to the onionlike shell structure of ionization [39] in which the intensity at the focus is higher and produces the higher charge states whereas the peak intensity away from the focus is less and only the lower charge states are ionized.

For the constant ion yield cut, one first interpolates the ion

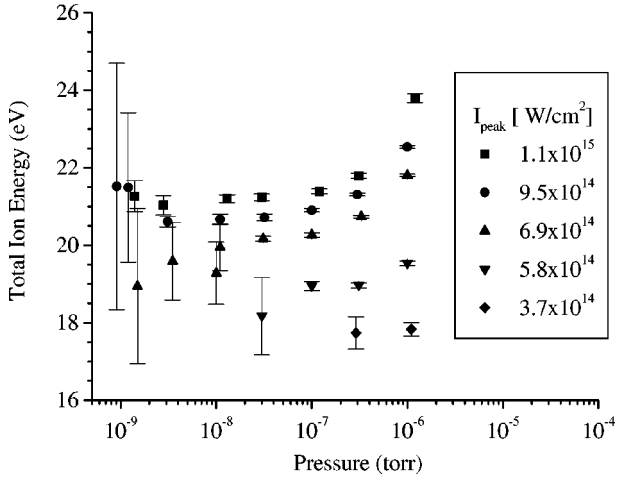

FIG. 4. Effects of space charge for the (3,1) dissociation channel. I_{peak} is the peak laser intensity at which the corresponding data were taken.

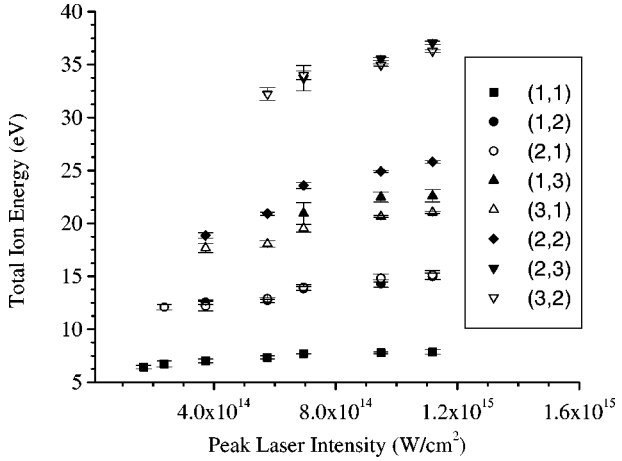

FIG. 5. Total ion energy for various dissociation channels of N_2 vs peak laser intensity.

yield curve to find the laser intensity which produces a specified ion yield (Fig. 6). One then interpolates the kinetic energy data (Fig. 5) for this laser intensity. Each cut of constant ion yield gives a single kinetic energy for each (n,m) dissociation. For analyzing dissociation pathways, one needs to use the high ion yield cut at the point where ionization has saturated. This is because each previous step in a given pathway must occur near saturation to have a significant population at the the end of the sequence.

To obtain R_{ion} for the energies from a particular cut, one needs a model for the relationship of observed kinetic energy to internuclear separation. Previous groups have determined R_{ion} [$R_{n,m}$ for the (n,m) channel] by equating the measured kinetic energy $E_{n,m}^{\text{meas}}$ with the potential energy curve for the (n,m) state, $V_{n,m}(R_{n,m})$:

$$E_{n,m}^{\text{meas}} = V_{n,m}(R_{n,m}) - V(\infty). \tag{9}$$

Note: from here on we will assume V has been adjusted so that $V(\infty)=0$. However, Eq. (9) does not take into account

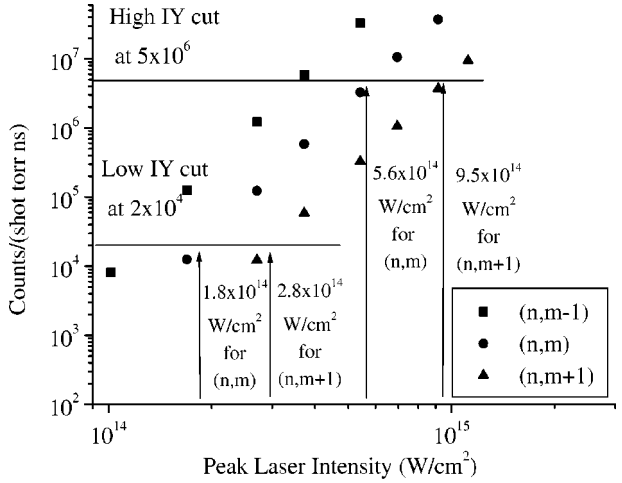

FIG. 6. Ion yields for a hypothetical data set with examples of high and low constant intensity cuts with the respective intensities for each channel.

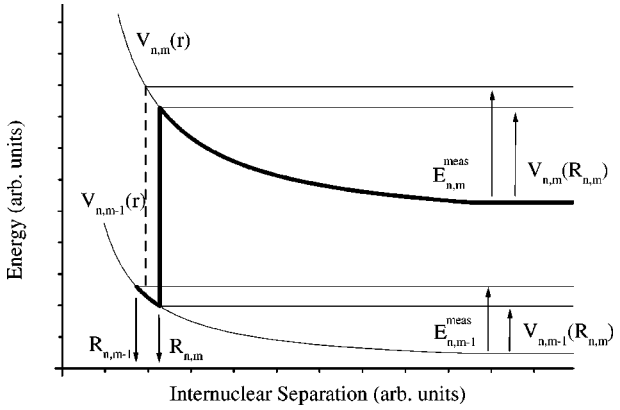

FIG. 7. Definition of terms for a pair of hypothetical potential energy curves.

the initial kinetic energy of the fragments gained before reaching the (n,m) charge state. Therefore, an additional term needs to be added, as was considered in Ref. [15]:

$$E_{n,m}^{\mathrm{meas}} = V_{n,m}(R_{n,m}) + E_{n,m}^{\mathrm{acc}}, \tag{10}$$

where $E_{n,m}^{\mathrm{acc}}$ is the accumulated kinetic energy from all previous ionization steps. The accumulated kinetic energy to the (n,m) dissociation is the sum of the accumulated kinetic energy up to the $(n,m-1)$ dissociation, $E_{n,m-1}^{\mathrm{acc}}$ plus the kinetic energy gained on the $(n,m-1)$ curve, $\triangle E_{n,m-1}$:

$$E_{n,m}^{\mathrm{acc}} = E_{n,m-1}^{\mathrm{acc}} + \triangle E_{n,m-1}. \tag{11}$$

$\triangle E_{n,m-1}$ is the added kinetic energy from traveling down the $V_{n,m-1}(r)$ potential energy curve from $R_{n,m-1}$ to $R_{n,m}$ (Fig. 7):

$$\triangle E_{n,m-1} = V_{n,m-1}(R_{n,m-1}) - V_{n,m-1}(R_{n,m}). \tag{12}$$

Similarly to Eq. (10), the measured kinetic energy from the $(n,m-1)$ dissociation is

$$E_{n,m-1}^{\mathrm{meas}} = E_{n,m-1}^{\mathrm{acc}} + V_{n,m-1}(R_{n,m-1}). \tag{13}$$

Solving for $E_{n,m-1}^{\mathrm{acc}}$ in Eq. (13) and substituting Eq. (11) and Eq. (12) into Eq. (10), we arrive at

$$E_{n,m}^{\mathrm{meas}} - E_{n,m-1}^{\mathrm{meas}} = V_{n,m}(R_{n,m}) - V_{n,m-1}(R_{n,m}). \tag{14}$$

Given the accumulation of kinetic energy from each previous ionization step, one might think that it is necessary to include the history of all previous steps. However, we see in Eq. (14) that the measured energy of the previous step $(n,m-1)$ contains the necessary information from *all* previous steps. By taking the difference of $E_{n,m}^{\mathrm{meas}}$ and $E_{n,m-1}^{\mathrm{meas}}$, we include only the added kinetic energy from the travel along $V_{n,m-1}$ from $R_{n,m-1}$ to $R_{n,m}$.

More generally, one can consider any sequential or nonsequential ionization step from (i,j) to (n,m). Therefore, the generalized form of Eq. (14) is

$$E_{n,m}^{\mathrm{meas}} - E_{i,j}^{\mathrm{meas}} = V_{n,m}(R_{n,m}) - V_{i,j}(R_{n,m}). \tag{15}$$

The only problem with Eq. (15) is that if the (i,j) channel does not dissociate, then one cannot use it to take into account its accumulated kinetic energy and this equation will not apply. In our results, N_2 and N_2^+ are bound so we will need to consider separately ionization to N_2^+ and N_2^{2+}.

Until now the potential energy curves, $V_{n,m}(r)$, have been discussed in only general terms. Most often Coulomb curves have been used in analyzing strong field molecular data. However, Coulomb curves do not take into account the complex binding nature of molecules at close (1–3 Å) internuclear separation. Actual molecular curves do take into account the binding nature but often only the dication or trication have been calculated in detail. In this work we use known curves when available and use an approximate binding contribution to the Coulomb curves for higher charge states.

If one assumes that the potential energy is a sum of a Coulomb repulsion term, $kq_1q_2/R_{n,m}$, and a bonding term, $V'_{n,m}(R_{n,m})$, the total potential energy is then

$$V_{n,m}(r) = k\frac{nm}{r} - V'_{n,m}(r). \tag{16}$$

We can rewrite Eq. (15) using Eq. (16):

$$E_{n,m}^{\mathrm{meas}} - E_{i,j}^{\mathrm{meas}} = k\frac{nm}{R_{n,m}} - V'_{n,m}(R_{n,m}) - \left(k\frac{ij}{R_{n,m}} - V'_{i,j}(R_{n,m}) \right) \tag{17}$$

$$= \frac{k(nm-ij)}{R_{n,m}} - \triangle V'(R_{n,m}), \tag{18}$$

where

$$\triangle V'(R_{n,m}) = V'_{n,m}(R_{n,m}) - V'_{i,j}(R_{n,m}). \tag{19}$$

As it turns out, the bonding contribution to the potential energy curves is relatively constant, even up to high charge states [40,41], and thus $\triangle V'(R_{n,m})$ is quite small. Assuming $\triangle V'(R_{n,m}) = 0$, Eq. (15) becomes particularly simple:

$$E_{n,m}^{\mathrm{meas}} - E_{i,j}^{\mathrm{meas}} = \frac{k(nm-ij)}{R_{n,m}}. \tag{20}$$

Equation (20) takes into account the accumulated kinetic energy and, approximately, the molecular binding in determining $R_{n,m}$. Given its simplicity, this expression could and should be used for all analysis of strong field molecular dissociation data when specific potential energy curves do not exist for Eq. (15).

Once one knows both $V_{n,m}(R_{n,m})$ and $R_{n,m}$, it is then possible to determine the time required to travel from one ionization step to the next. The equation of motion is

$$\frac{1}{4}m\left(\frac{dr}{dt}\right)^2 + V(r) = E_{\mathrm{total}}, \tag{21}$$

where r is the internuclear separation. Equation (21) can be solved for the time it takes to travel from $R_{i,j}$ to $R_{n,m}$ on the $V_{i,j}(r)$ potential energy curve, $T_{ij\to nm}$:

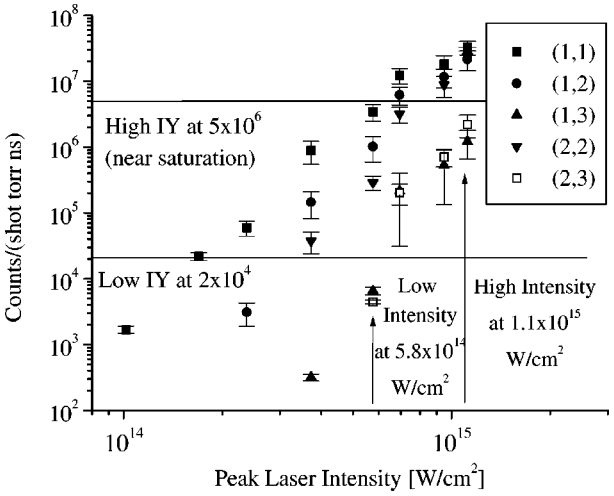

FIG. 8. Ion yields for observed channels.

$$T_{ij\to nm}=\int_{R_{i,j}}^{R_{n,m}}\frac{dr}{\sqrt{\frac{4}{m}[V_{i,j}(R_{i,j})-V_{i,j}(r)]}} \qquad (22)$$

and can be integrated numerically for any arbitrary potential, $V_{i,j}(r)$.

V. ACTUAL IONIZATION PATHWAYS

The analysis presented in Sec. IV can be applied to our measured dissociation energies (Fig. 5). For constant laser intensity cuts we have chosen 5.8×10^{14} W/cm^2 and 1.1×10^{15} W/cm^2 for the low and high cuts, respectively. Constant ion yield cuts are determined from Fig. 8 using 5×10^6 and 2×10^4 counts/(shot torr ns) as the high and low ion yields, respectively. The high cut was taken at saturation and the low cut was taken at the lowest ion yield where sufficient statistics were available, i.e., at threshold. The results of these different cutting methods are summarized in Fig. 9.

To convert the data in Fig. 9 to internuclear separation, we need potential energy curves as discussed in the previous section. The curves for N_2, N_2^+, N_2^{2+}, and N_2^{3+} are known (Fig. 10) [42–45]. Thus, for N_2^{3+} we can use Eq. (15) directly. For N_2^{4+} and N_2^{5+} we use Eq. (20), which approximately takes into account the bonding contribution to these charge states. However, as discussed above, we must separately consider the ionization to N_2^+ and N_2^{2+}.

In our experiments diatomic nitrogen starts in its ground state. We see that the overlap of the ground state (N_2) with the lowest level of the single ionized state is extremely good (Fig. 10), so that there is very little change in internuclear separation through ionization from N_2 to N_2^+. While we observe both the N_2^+ and the (1,0) dissociation channel the (1,0) channel is small and probably arises from bond softening, but does not significantly contribute to the rest of the ionization pathways. The first important dissociation channel is the (1,1) channel. In this case Eq. (15) cannot be used because the previous steps (N_2, N_2^+) do not dissociate. Using the Coulombic approximation for $V_{1,1}(R_{1,1})$ in Eq. (9) for the (1,1) dissociation gives $R_{1,1}=1.97$ Å, almost twice the equilibrium internuclear separation ($R_E=1.1$ Å). As discussed above in Sec. I, this abrupt change in internuclear separation from R_E has not been adequately explained. However, this problem is simply resolved by considering the known curves of N_2^{2+} (Fig. 11).

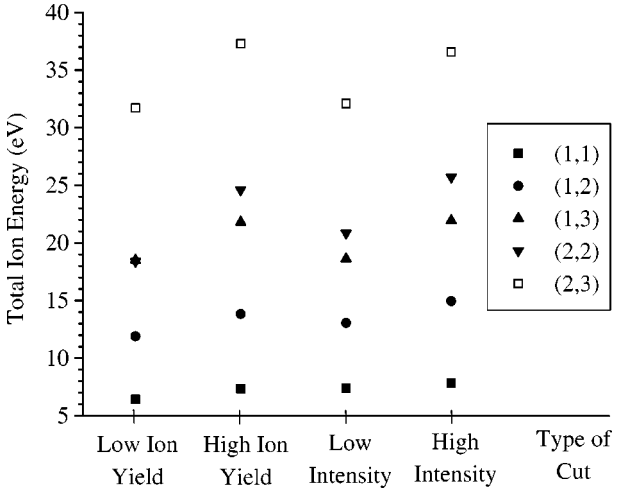

FIG. 9. Two measurements at constant laser intensity and two at constant ion yield. Data for (1,2) and (2,1), (1,3) and (3,1), and (2,3) and (3,2) have been averaged for the (1,2), (1,3), and (2,3) results, respectively.

The population of N_2^+ is at a potential minimum at R_E such that further ionization up to N_2^{2+} through a vertical transition leaves the population at R_E. N_2^{2+} is populated into two catagories: dissociating and bound. For the (1,1) channel, measured energies range from 6.8 eV (low intensity, 2.4×10^{14} W/cm^2) to 7.9 eV (high intensity, 1.1×10^{15} W/cm^2). Plotting this range of energies over the actual curves in Fig. 11, we see that many states are consistent with ionization at R_E. It is important to note that we do not need to consider the prior accumulation of kinetic energy in Eq.

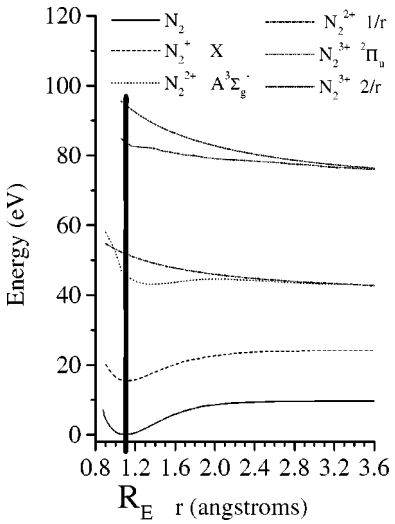

FIG. 10. Potential energy curves for N_2, N_2^+, N_2^{2+}, and N_2^{3+} from Refs. [42–45].

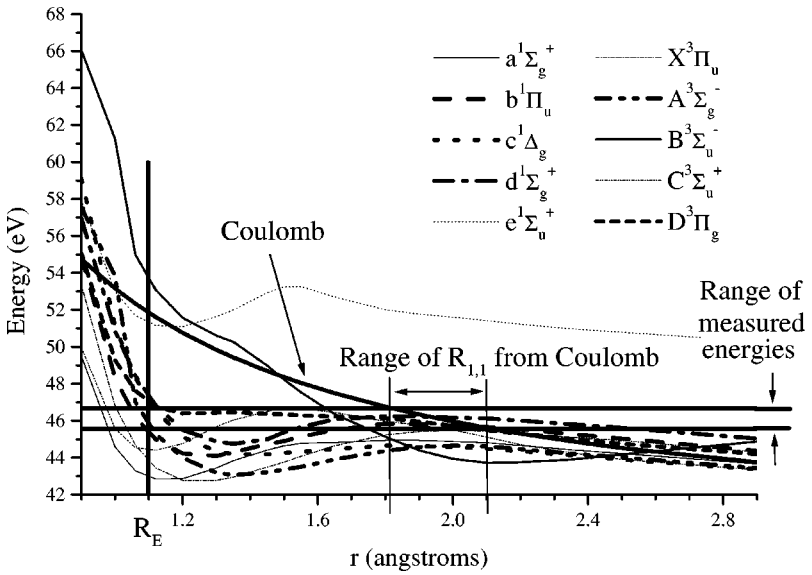

FIG. 11. N_2^{2+} potential energy curves from Refs. [43,44]. Zero energy corresponds to $N_2(\nu=0)$. Thick traces correspond to possible dissociative curves whereas thin traces correspond to bound curves at R_E. Also included is the purely Coulombic curve. The range of $R_{1,1}$ is inferred from the Coulomb curve from our range of measured energies.

(10) since N_2^+ is not vibrationally excited and has started at R_E. Comparing these energies to the field-free curves of Fig. 11, we see that a number of bound and dissociating states are populated. With the exception of the $B^3\Sigma_u^-$ state, every state is either bound at R_E or dissociates with a kinetic energy that is consistent with what is observed in our experiments. Thus, it is quite reasonable to assume that the lowest energy dissociating state for N_2^{2+} is the $A\,^3\Sigma_g^-$, and is produced near R_E with no kinetic energy.

We can now determine $R_{\rm ion}$ along various pathways since we have well-defined initial conditions for the (1,1) channel using Eq. (15). There are two considerations for determining ionization pathways: does the ionization produce symmetric or asymmetric charge distributions, and is the ionization one-electron (sequential) or multielectron (nonsequential)? These possibilities are shown in Eqs. (23)–(28):

$$(1,1)\rightarrow(1,2)\rightarrow(2,2)\rightarrow(2,3),\quad 1e^-,\ \text{symmetric,} \tag{23}$$

$$(1,1)\rightarrow(1,2)\rightarrow(1,3)\rightarrow(2,3),\quad 1e^-,\ \text{asymmetric,} \tag{24}$$

$$(1,1)\rightarrow(1,2)\rightarrow(2,3),\quad 2e^-,\ \text{symmetric,} \tag{25}$$

$$(1,1)\rightarrow(2,2)\rightarrow(2,3),\quad 2e^-,\ \text{symmetric,} \tag{26}$$

$$(1,1)\rightarrow(1,3)\rightarrow(2,3),\quad 2e^-,\ \text{asymmetric,} \tag{27}$$

$$(1,1)\rightarrow(2,3),\quad 3e^-,\ \text{symmetric.} \tag{28}$$

$R_{n,m}$ for each step can be found for Eqs. (23)–(28) using Eqs. (15) and (20) and the dissociation energies from Fig. 9. Table I provides a summary of the high ion yield energies for the above pathways, the most relevant cut for analyzing dissociation pathways. For completeness we also give the results for the other cuts in Table II. A basic physical assumption is that $R_{n,m}$ must strictly increase along a given pathway. As seen in Table I, this is not always the case.

VI. DISCUSSION

Figure 12 is a plot of the results from Table I for the symmetric and asymmetric sequential pathways. Also plotted is $R_{\rm ion}$ using the Coulomb model, $E=kq_1q_2/R_{\rm ion}$, for both the symmetric and asymmetric dissociations.

On the one hand, Fig. 12 shows that the Coulomb model gives rise to a nearly constant value of $\sim$2.2 Å for the internuclear separation, $R_{\rm ion}$. This is consistent with previous work on N_2 and led to the identification of critical internuclear separation, R_C. However, a physical mechanism to get

TABLE I. High ion yield cut for 33 fs data. Included are pathway description, internuclear separation for each step along a path, and whether or not the pathway is consistent with the previous step.

Pathway		$R_{n,m}$ (Å)	Consistent with previous step?
	(1,1)	1.08	starting point
	(1,1) → (1,2)	1.70	Yes
	(1,2) → (2,2)	2.67	Yes
$1e^-$ sym	(2,2) → (2,3)	2.27	No
	(1,1) → (1,2)	1.70	Yes
	(1,2) → (1,3)	1.80	Yes
$1e^-$ asym	(1,3) → (2,3)	2.79	Yes
	(1,1) → (2,2)	2.29	Yes
$2e^-$ sym	(2,2) → (2,3)	2.27	No
	(1,1) → (1,2)	1.70	Yes
$2e^-$ sym	(1,2) → (2,3)	0.61	No
	(1,1) → (1,3)	1.75	Yes
$2e^-$ asym	(1,3) → (2,3)	2.79	Yes
$3e^-$ sym	(1,1) → (2,3)	2.28	Yes

TABLE II. Low ion yield and low (5.8×10^{14} W/cm^2) and high (1.1×10^{15} W/cm^2) intensity table for 33 fs data. Also indicated is whether each step is consistent with the previous.

	Low IY		Low intensity		High intensity	
path	$R_{n,m}$ (Å)	Consistent	$R_{n,m}$ (Å)	Consistent	$R_{n,m}$ (Å)	Consistent
(1,1)	1.13	start	1.08	start	1.07	start
(1,1) → (1,2)	1.86	Yes	1.84	Yes	1.63	Yes
(1,2) → (2,2)	4.43	Yes	3.69	Yes	2.68	Yes
(2,2) → (2,3)	2.16	No	2.56	No	2.64	No
(1,1) → (1,2)	1.86	Yes	1.84	Yes	1.63	Yes
(1,2) → (1,3)	2.18	Yes	2.59	Yes	2.06	Yes
(1,3) → (2,3)	3.27	Yes	3.20	Yes	2.95	Yes
(1,1) → (2,2)	3.45	Yes	3.07	Yes	2.18	Yes
(2,2) → (2,3)	2.16	No	2.56	No	2.64	Yes
(1,1) → (1,2)	1.86	Yes	1.84	Yes	1.63	Yes
(1,2) → (2,3)	0.60	No	0.59	No	.60	No
(1,1) → (1,3)	2.00	Yes	2.19	Yes	1.78	Yes
(1,3) → (2,3)	3.27	Yes	3.20	Yes	2.95	Yes
(1,1) → (2,3)	2.75	Yes	2.83	Yes	2.38	Yes

from R_E to R_C for the (1,1) channel has still not been identified. On the other hand, our results using Eqs. (15) and (20) show a very different picture. First, our analysis removes the problem of the initial expansion of the molecule: the (1,1) channel starts near R_E and the subsequent expansion of the molecule occurs on repulsive curves. No new physics is needed to explain the increase in internuclear separation. The second important observation from Fig. 12 is that the internuclear separation for the creation of the (2,3) from the symmetric dissociation [Eq. (23))] is at a smaller internucluear separation than for the creation of the previous step, (2,2). Since it is quite unlikely that the internuclear separation will actually decrease during dissociation, the symmetric one-electron path to the (2,3) channel is unphysical. This is in stark contrast to the asymmetric pathway [Eq. (24)] in which the internuclear separation of all the channels increases monatomically, as would be expected. This leads to the startling conclusion that the symmetric pathway terminates at (2,2) and does not lead to higher charge states. Conversely, all ionization up to N_2^{5+} appears to proceed through the asymmetric channel. Finally, these results definitively show that the asymmetric channel (1,3) is created at a smaller internuclear separation than the symmetric channel, as suggested by other groups [5,27] using only the Coulomb model.

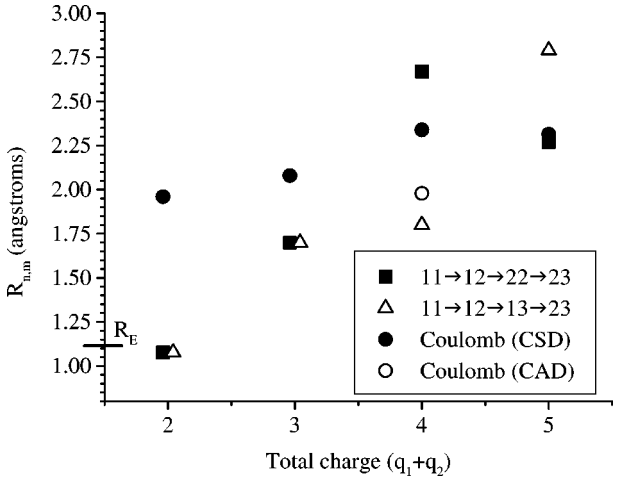

FIG. 12. $R_{n,m}$ for the one-electron symmetric and asymmetric ionization pathways. Also shown are the charge symmetric dissociation (CSD) and charge asymmetric dissociation (CAD) from the Coulomb model, which do not take into account previous ionization history and hence are not complete pathways.

Similar conclusions hold for nonsequential channels: the asymmetric channels are consistent, while the symmetric channels are not. However, we have no basis to judge the relative strength or importance of the nonsequential pathways as compared to the sequential pathways.

Although we believe the high ion yield data to be the correct cut to use for analyzing ionization pathways, we tested the sensitivity of our results to the cutting method, shown in Table II. Even though the specific value of $R_{n,m}$ change somewhat with the type of cut, the more important question of consistency in the expansion of the molecule remains unchanged. Thus, our conclusions appear to be robust.

Given this insensitivity to the cutting method, we can reanalyze previously published data (100 fs, 600 fs, and 2 ps)

TABLE III. Comparison of $R_{n,m}$ for 100 fs, 600 fs, and 2 ps pulse durations from Ref. [2]. Also indicated is whether each step is consistent with the previous.

	100 fs		600 fs		2 ps	
path	$R_{n,m}$ (Å)	Consistent	$R_{n,m}$ (Å)	Consistent	$R_{n,m}$ (Å)	Consistent
(1,1)	1.10	start	1.15	start	1.09	start
(1,1) → (1,2)	1.73	Yes	1.64	Yes	1.95	Yes
(1,2) → (2,2)	3.23	Yes	3.20	Yes	3.60	Yes
(2,2) → (2,3)	2.88	No	3.60	Yes	3.60	Yes
(1,1) → (1,2)	1.73	Yes	1.64	Yes	1.95	Yes
(1,2) → (1,3)	2.44	Yes	2.05	Yes	2.40	Yes
(1,3) → (2,3)	3.32	Yes	4.32	Yes	4.32	Yes
(1,1) → (2,2)	2.69	Yes	2.52	Yes	3.18	Yes
(2,2) → (2,3)	2.88	No	3.60	Yes	3.60	Yes
(1,1) → (1,2)	1.73	Yes	1.64	Yes	1.95	Yes
(1,2) → (2,3)	0.59	No	0.59	No	0.58	No
(1,1) → (1,3)	1.98	Yes	1.80	Yes	2.28	Yes
(1,3) → (2,3)	3.32	Yes	4.32	Yes	4.32	Yes
(1,1) → (2,3)	2.77	Yes	2.93	Yes	3.35	Yes

[2] using Eqs. (15) and (20) with some confidence without knowing all the experimental details. These results are shown in Table III.

It is important to note that if the pulse duration is greater than 100 fs, all pathways are possible. This implies that the dissociation pathways are a function of laser pulse duration. As the field is on longer, both symmetric as well as asymmetric pathways are possible.

Given the robustness and consistency of our analysis, the question of why the symmetric pathway terminates for short laser pulses but not for long pulses becomes quite significant. To answer this, we looked at the time between each ionization step for 33 fs and 600 fs [2] pulse durations using Eq. (22). For our 33 fs data, we have measured the saturation intensity for each channel so we can plot these intensities against the timing of the channels to produce a complete picture of the ionization process, Fig. 13. Also plotted in Fig. 13 is a Gaussian pulse of 33 fs full width at half maximum (FMHM) with the height set by the maximum laser intensity used for our experiment. For comparison, timing of the channels of our data for 33 fs and data of Cornaggia *et al.* for 600 fs [2] have been plotted in Fig. 14 as a function of laser intensity. For the 600 fs data, we have plotted a Gaussian pulse of 600 fs FWHM with the height set by the maximum laser intensity used for the 33 fs experiment. For the 600 fs data, saturation intensities were not reported so we have fixed the data to lie on the Gaussian envelope with the starting ionization point for the (1,1) channel at the same intensity as the 33 fs data.

As expected for the 33 fs pulse in Fig. 13, the ionization starts on the rising edge of the pulse, where the (1,1) and (1,2) channels are produced. At the next step the two pathways diverge. Apparently, the rising intensity is not sufficient to ionize the $(1,2)\rightarrow(2,2)$. Rather, the molecule needs to approach R_C for the enhancement in the ionization rate at this point. In contrast, the (1,3) channel appears to be more strongly governed by rising intensity than R_C enhancement. This implies that as a function of intensity, the rate from $(1,2)\rightarrow(1,3)$ greatly exceeds that of $(1,2)\rightarrow(2,2)$. For this reason, the $(1,2)\rightarrow(2,2)$ ionization channel is effected little by the peak laser intensity and needs to approach R_C for enhanced ionization and is only reached on the falling edge

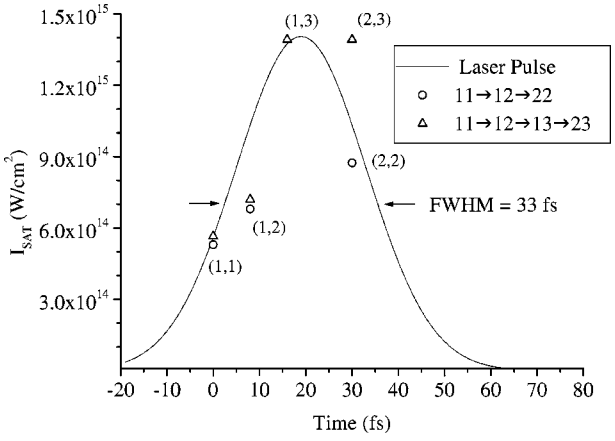

FIG. 13. Comparison of time between ionization steps for data from Table I to a 33 fs duration Gaussian. I_{sat} is the saturation intensity for each channel. For clarity, individual channels have been labeled.

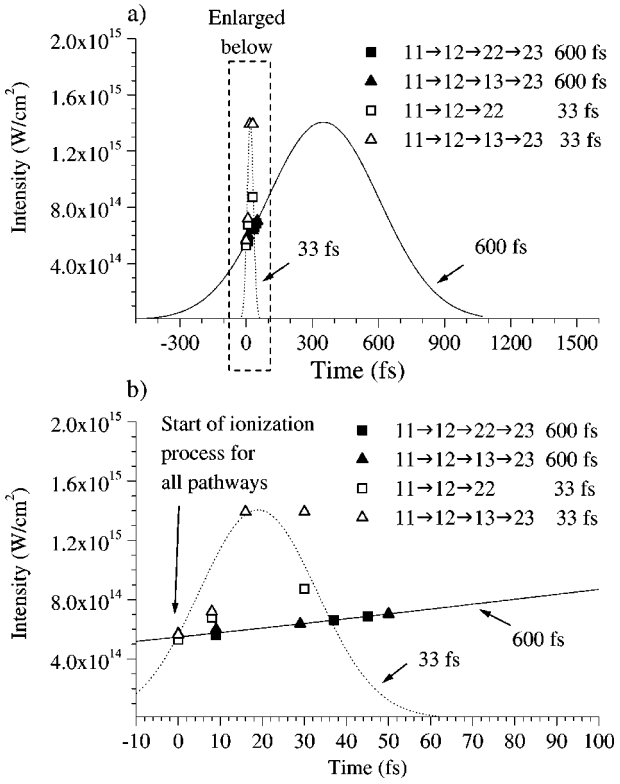

FIG. 14. Comparison of time between ionization steps for high IY (from Table I) and 600 fs (from Table III) to 33 fs and 600 fs Gaussian envelopes.

of the 33 fs laser pulse. Since (2,2) is created in a decreasing laser intensity, no further ionization along the sequential symmetric pathway is possible.

Alternatively, the (2,2) channel may not be produced by ionization at all. It has been noted [5,29] that the asymmetric channels, like the (1,3), are electronically excited over the symmetric ground state, e.g., the (2,2). Because of this, as the asymmetric channel expands, it will encounter numerous curve crossings with excited states of the symmetric channel. The (1,3) channel can convert to an excited state $(2,2)^*$ channel during dissociation. Thus, our results are consistent with previous observations that strong field ionization by short laser pulses, 33 fs [9] and 60 fs [10], can leave the atomic fragments in excited states. If this is, in fact, the origin of the (2,2) channel, the (1,3) channel would have to be created at a smaller internuclear separation than the (2,2), which is precisely what we observe. The (1,3) is created at 1.80 Å , which expands to the observed separation of 2.67 Å for the creation of the (2,2) channel. At this point there can be a curve crossing of the (1,3) and the $(2,2)^*$ potential energy curves [5].

The situation is different for long pulse durations, as can be seen in Fig. 14. Here, because the change in intensity is much slower, the ionization is dominated by the enhanced ionization as the internuclear separation expands to R_C. As compared to the short pulse, the (2,2) now has time to expand to R_C and hence it undergoes ionization to (2,3) on the rising edge of the pulse. The observation of (1,3) for long pulse durations brings up many issues. If no (1,3) channel was seen for long pulse durations, but was only seen for short pulse durations, then we could conclude that its ionization is dominated solely by intensity. However, the (1,3) channel is seen at long pulse durations in which the laser intensity rise time is slow. Thus, there may be some R_C enhancement for asymmetric dissociation as well. However, R_C enhancement has never been investigated theoretically for asymmetric dissociations.

Comparing results of the 33 fs to 600 fs pulses, we see that there are two quantifiable differences: laser intensity rise time and ionization pathways. Laser intensity rise time allows us to distinguish between ionization dominated by intensity (fast rise time, 33 fs) or by R_C enhancement (slow rise time, 600 fs). Secondly, the only ionization pathway for 33 fs is the asymmetric pathway, whereas both asymmetric and symmetric pathways are possible for 600 fs. Therefore, intensity-dominated ionization gives rise to an asymmetric pathway whose fragments may be different than the fragments of the asymmetric pathway created from R_C enhancement. We hypothesize that intensity-dominated asymmetric pathways leave the fragments in electronically excited states and that R_C enhanced symmetric and asymmetric pathways leave fragments in their electronic ground state.

These results for short and long pulse durations shed new light on another long-standing puzzle in the strong-field ionization of molecules: the observation that highly charged highly unstable molecules, such as Cl_2^{6+}, do not appear to dissociate until the end of the laser pulse, i.e., the molecule is stabilized against dissociation by the laser field [31,32]. Schmidt *et al.* were led to this conclusion by the absence of any significant ionization of the molecular fragments following dissociation, referred to as postdissociation ionization (PDI), using 2 ps laser pulses. With this relatively long pulse duration, they assumed that there should be sufficient time to ionize the atomic fragments later in the pulse. To confirm the fact that ionization should occur if the molecule has dissociated, they repeated the experiment with two 100 fs pulses separated by 1.4 ps. Under these conditions, there is no mechanism for stabilizing the molecules between the laser pulses and, indeed, PDI was seen to be induced by the second laser pulse. Thus, it appeared that with 2 ps laser pulses, the molecule really does not dissociate while the field is on, preventing any PDI.

Given our results and recent observations on molecules in strong fields, we propose an alternative explanation for the stabilization experiments. Schmidt *et al.* assumed that the electronic state of the dissociation fragments following strong-field ionization was the same for the short and long laser pulses. However, it is becoming increasing clear that short pulse (<100 fs) ionization leaves the fragments in excited states [9,10]. With their smaller ionization potentials, these excited-state fragments will be more easily ionized by the laser field. It is quite possible that the presence of PDI with the two short laser pulses was a consequence of the fragments being in excited states. In the experiments with long laser pulses, the fragments were left in their ground state and never experienced a high enough intensity to ionize. Thus, the stabilization experiments can be explained by

the short pulse leaving fragments in excited states, rather than by the long pulse stabilizing the molecule.

VII. CONCLUSION

In this paper, we have studied the ionization and dissociation pathways of N_2 with a strong laser field. Considering the accumulated kinetic energy and non-Coulombic potential energy curves, we have come to the following conclusions. (i) Ionization does not simply occur at a critical internuclear separation, as has been previously reported, but rather, the molecule steadily expands on repulsive potential curves starting from its equilibrium separation. (ii) The charge asymmetric channel (1,3) is definitely produced at a smaller separation than its symmetric counterpart (2,2). This observation opens the possibility that the (3,1) channel can covert to an excited state $(2,2)^*$ channel through a curve crossing in the N_2^{4+} charge state providing a mechanism for the generation of excited-state fragments that have been seen in recent experiments. Perhaps more significantly, the smaller separation for the (3,1) channel shows that the asymmetric channel *cannot* be formed by a charge transfer from the (2,2) channel, as has been previously proposed [29,46]. This, once again, leaves completely open the origin of the asymmetric channels. (iii) With 33 fs laser pulses, all ionization proceeds through the asymmetric channel, reinforcing the idea that the (2,2) is a byproduct of the (3,1) channel. (iv) We observe the competition between intensity-dominated and internuclear separation-dominated ionization rates, the former applying to short pulses, the latter to long pulses. (v) Taken together, these results suggest a new interpretation of strong-field stabilization experiments that does not need a stabilization mechanism.

ACKNOWLEDGMENTS

We would like to acknowledge support from the NSF under Grant No. NSF-PHYS-9987804. G.N.G. was also supported by the Research Corporation.

[1] K. Codling, C. Cornaggia, L.J. Frasinski, P.A. Hatherly, J. Morellec, and D. Normand, J. Phys. B **24**, L593 (1991).
[2] C. Cornaggia, J. Lavancier, D. Normand, J. Morellec, P. Agostini, J.P. Chambaret and A. Antonetti, Phys. Rev. A **44**, 4499 (1991).
[3] C. Cornaggia, J. Lavancier, D. Normand, J. Morellec, and H.X. Liu, Phys. Rev. A **42**, 5464 (1990).
[4] J.H. Posthumus, K. Codling, L.J. Frasinski, and M.R. Thompson, Laser Phys. **7**, 813 (1997).
[5] G.N. Gibson, M. Li, C. Guo, and J.P. Nibarger, Phys. Rev. A **58**, 4723 (1998).
[6] B. Friedrich and D. Herschbach, Phys. Rev. Lett. **74**, 4623 (1995).
[7] H. Stapelfeldt, Hirofumi Sakai, E. Constant, and P.B. Corkum, Phys. Rev. Lett. **79**, 2787 (1997).
[8] J. Karczmarek, J. Wright, P.B. Corkum, and M. Yu Ivanov, Phys. Rev. Lett. **82**, 3420 (1999).
[9] J.P. Nibarger, M. Li, S. Menon, and G.N. Gibson, Phys. Rev. Lett. **83**, 4975 (1999).
[10] L. Quaglia and C. Cornaggia, Phys. Rev. Lett. **84**, 4565 (2000).
[11] T. Seideman, M. Yu. Ivanov, and P.B. Corkum, Phys. Rev. Lett. **75**, 2819 (1995).
[12] R. Barnett and G.N. Gibson, Phys. Rev. A **59**, 4843 (1999).
[13] A.D. Bandrauk and Y. Hengtai, Int. J. Mass Spectrom. Ion Processes **192**, 379 (1999).
[14] A. Saenz, Phys. Rev. A **61**, 051402(R) (2000).
[15] S. Chelkowski and A.D. Bandrauk, J. Phys. B **28**, L723 (1995).
[16] T. Zuo and A.D. Bandrauk, Phys. Rev. A **52**, R2511 (1995).
[17] T. Zuo, S. Chelkowski, and A.D. Bandrauk, Phys. Rev. A **48**, 3837 (1993).
[18] A.D. Bandrauk, in *The Physics of Electronic and Atomic Collisions*, edited by Y. Itikawa, K. Okuno, H. Tanaka, A. Yagishita, and M. Matsuzawa, AIP Conf. Proc. No. 500 (AIP, New York, 2000), p. 102.
[19] U. Eichmann, M. Dorr, M. Maeda, W. Becker, and W. Sandner, Phys. Rev. Lett. **84**, 3550 (2000).
[20] E. Constant, H. Stapelfeldt, and P.B. Corkum, Phys. Rev. Lett. **76**, 4140 (1996).
[21] G.N. Gibson, M. Li, C. Guo, and J. Neira, Phys. Rev. Lett. **79**, 2022 (1997).
[22] A. Zavriyev, P.H. Bucksbaum, H.G. Muller, and D.W. Schumacher, Phys. Rev. A **42**, 5500 (1990).
[23] A. Zavriyev, P.H. Bucksbaum, J. Squier, and F. Saline, Phys. Rev. Lett. **70**, 1077 (1993).
[24] M. Brewczyk, K. Rzazewski, and Charles W. Clark, Phys. Rev. Lett. **78**, 191 (1997).
[25] M. Brewczyk and K. Rzazewski, Phys. Rev. A **60**, 2285 (1999).
[26] M. Brewczyk and K. Rzazewski, Phys. Rev. A **61**, 023412 (2000) (''energy deficit'' refers to the difference in dissociation energy for ionization occurring at R_E using Coulomb curves and the measured energy).
[27] A. Iwamae, A. Hishikawa, and K. Yamanouchi, J. Phys. B **33**, 223 (2000).
[28] I. Kawata, H. Kono, Y. Fujimura, and A.D. Bandrauk, Phys. Rev. A **62**, 031401(R) (2000).
[29] D.T. Strickland, Y. Beaudoin, P. Dietrich, and P.B. Corkum, Phys. Rev. Lett. **68**, 2755 (1992).
[30] A. Hishikawa, A. Iwamae, K. Hoshina, M. Kono, and K. Yamanouchi, Chem. Phys. Lett. **282**, 283 (1998).
[31] M. Schmidt, D. Normand, and C. Cornaggia, Phys. Rev. A **50**, 5037 (1994).
[32] M. Schmidt, P. D'Oliveira, P. Meynadier, D. Normand, and C. Cornaggia, J. Nonlinear Opt. Phys. Mater. **4**, 817 (1995).
[33] B. Walker, B. Sheehy, L.F. DiMauro, P. Agostini, K.J. Schafer, and K.C. Kulander, Phys. Rev. Lett. **73**, 1227 (1994).
[34] W.T. Hill, J. Zhu, D.L. Hatten, Y. Cui, J. Goldhar, and S. Yang, Phys. Rev. Lett. **69**, 2646 (1992).
[35] M. Li and G.N. Gibson, J. Opt. Soc. Am. B . **15**, 2404 (1998)

[36] C. Guo, M. Li, J.P. Nibarger, and G.N. Gibson, Phys. Rev. A **58**, R4271 (1998).
[37] A. Hishikawa, A. Iwamae, K. Hoshina, M. Kono, and K. Yamanouchi, Chem. Phys. **231**, 315 (1998).
[38] K. Boyer, T.S. Luk, J.C. Solem, and C.K. Rhodes, Phys. Rev. A **39**, 1186 (1989).
[39] M. Schmidt, S. Dobosz, P. Meynadier, P. D'Oliveira, D. Normand, E. Charron, and A. Suzor-Weiner, Phys. Rev. A **60**, 4706 (1999).
[40] P.B. Corkum, M.Yu Ivanov, and J.S. Wright, Annu. Rev. Phys. Chem. **48**, 387 (1997).
[41] J.S. Wright, G.A. DiLabio, D.R. Matusek, P.B. Corkum, M. Yu Ivanov, Ch. Ellert, R.J. Buenker, A.B. Alekseyev, and G. Hirsch, Phys. Rev. A **59**, 4512 (1999).
[42] A. Lofthus and P.H. Krupenie, J. Phys. Chem. Ref. Data **6**, 1 (1977).
[43] E.W. Thulstrup and A. Andersen, J. Phys. B **8**, 965 (1975).
[44] R.W. Wetmore and R.K. Boyd, J. Phys. Chem. **90**, 5540 (1986).
[45] A.D. Bandrauk, D.G. Musaev, and K. Morokuma, Phys. Rev. A **59**, 4309 (1999).
[46] P. Dietrich, D.T. Strickland, and P.B. Corkum, J. Phys. B **26**, 2323 (1993).